JVI Journals.ASM.org

Relationship between within-Host Fitness and Virulence in the Vesicular Stomatitis Virus: Correlation with Partial Decoupling

Victoria Furió,[a]* Raquel Garijo,[a] María Durán,[a] Andrés Moya,[a,b,c] John C. Bell,[d,e] and Rafael Sanjuán[a,b]

Institut Cavanilles de Biodiversitat i Biologia Evolutiva, Universitat de València, Spain[a]; Departament de Genètica, Universitat de València, Spain[b]; Unidad Mixta de Investigación en Genómica y Salud, Centro Superior de Investigación en Salud Pública (CSISP), Spain[c]; Cancer Therapeutics, Ottawa Hospital Research Institute, Ottawa, Ontario, Canada[d]; and Department of Medicine, University of Ottawa, Ottawa, Ontario, Canada[e]

Given the parasitic nature of viruses, it is sometimes assumed that rates of viral replication and dissemination within hosts (within-host fitness) correlate with virulence. However, there is currently little empirical evidence supporting this principle. To test this, we quantified the fitness and virulence of 21 single- or double-nucleotide mutants of the vesicular stomatitis virus in baby hamster kidney cells (BHK-21). We found that, overall, these two traits correlated positively, but significant outliers were identified. Particularly, a single mutation in the conserved C terminus of the N nucleocapsid (U1323A) had a strongly deleterious fitness effect but did not alter or even slightly increased virulence. We also found a double mutant of the M matrix protein and G glycoprotein (U2617G/A3802G mutant) with high fitness yet low virulence. We further characterized these mutants in primary cultures from mouse brain cells and *in vivo* and found that their relative fitness values were similar to those observed in BHK-21 cells. The mutations had weak effects on the virus-induced death rate of total brain cells, although they specifically reduced neuron death rates. Furthermore, increased apoptosis levels were detected in neurons infected with the U2617G/A3802G mutant, consistent with its known inability to block interferon secretion. *In vivo*, this mutant had reduced virulence and, despite its low brain titer, it retained a relatively high fitness value owing to its ability to suppress competitor viruses. Overall, our results are in broad agreement with the notion that viral fitness and virulence should be positively correlated but show that certain mutations can break this association and that the fitness-virulence relationship can depend on complex virus-host and virus-virus interactions.

Since viral replication takes place at the expense of host resources, it is often believed that, for a given virus, genetic variants showing faster replication and higher viral loads should tend to produce more-severe disease and higher mortality rates. This general principle could be experimentally tested by measuring within-host fitness and virulence for several genetic variants of a virus and determining whether these two variables correlate positively. This could help us to better understand the nature of virus-host interactions, pathogenesis, and viral epidemiology (1, 13) and may have practical implications as well. For instance, lower virulence often implies extended host survival times, and this may favor the virus by increasing its transmission opportunities, but on the other hand, competition among viral strains should favor those with higher within-host fitness. Therefore, if within-host fitness and virulence can be partially decoupled, viruses experiencing long evolutionary relationships with their hosts should tend to become less virulent over time. Also, it is well acknowledged that viral genetic variability at the population level depends on the spontaneous mutation rate, the fitness effects of mutations, the effective population size, or host ecology, among other factors (11), but the fate of new mutations should also be determined by how they affect virulence, inasmuch as virulence determines transmissibility. Finally, vaccine strains and viruses designed for therapeutic applications, such as oncolytic viruses, for instance, should ideally spread rapidly within hosts while retaining minimal virulence.

The principle that within-host fitness correlates with virulence is supported by the observation that serially passaged microorganisms tend to become more virulent in the host in which they have been passaged (12). Conversely, live attenuated viral vaccines generally have low fitness (26, 44). Also, a positive association between viral load in blood and disease progression has been established for HIV-1 (14). However, experimental determinations of within-host fitness and virulence in cucumber etch viruses infecting *Arabidopsis* supported a positive correlation but only for specific virus-host pairs (34). Analysis of a panel of single-nucleotide mutants of the tobacco etch virus showed no association between within-host fitness and virulence under controlled greenhouse conditions (5), similar to previous results obtained with the barley stripe mosaic virus (40). In the foot-and-mouth disease virus, the accumulation of mutations produced by serial plaque-to-plaque passages in cell cultures negatively impacts fitness, but the effects on virulence were found to be milder, suggesting that these two traits can be partially decoupled (21). Therefore, available empirical evidence provides mixed evidence for the correlation between within-host fitness and virulence.

Here, we quantified fitness and virulence in the standard cell line BHK-21 for 21 single- or double-nucleotide mutants of the vesicular stomatitis virus (VSV). We found that, overall, the data supported a positive correlation between these two traits, but significant outliers were found. Specifically, a mutation

Received 27 March 2012 **Accepted** 22 August 2012
Published ahead of print 5 September 2012
Address correspondence to Rafael Sanjuán, rafael.sanjuan@uv.es.
* Present address: Victoria Furió, Department of Zoology, University of Oxford, Oxford, United Kingdom.
V. F. and R.G. contributed equally to this article.

doi:10.1128/JVI.00755-12

TABLE 1 VSV mutants, cytotoxicity, and fitness in BHK-21 cells

Genome site of substitution[a]	Mutated gene	Amino acid substitution	Value (avg ±SEM) for relative:		Type of mutation or reference[b]
			Cytotoxicity	Fitness	
U906C	N	None	1.100 ± 0.042	1.055 ± 0.021	Random
U1323A	N	F420L	1.153 ± 0.018	0.429 ± 0.024	Random
G1544A	P	R50K	0.972 ± 0.035	1.032 ± 0.016	15
U1820C	P	I142T	0.981 ± 0.042	0.737 ± 0.028	7
G2344A	M	S32N	1.063 ± 0.023	1.032 ± 0.011	18, 29
C2608A	M	P120G	1.072 ± 0.028	0.779 ± 0.017	7
U2617G	M	L123W	1.019 ± 0.030	1.148 ± 0.033	32
A3120U	G	N15Y	0.950 ± 0.022	0.908 ± 0.027	3
A3802G	G	H242R	1.169 ± 0.030	1.160 ± 0.032	7
A4179G	G	T368A	0.838 ± 0.018	0.731 ± 0.019	7
G4459U	G	W461L	0.981 ± 0.026	0.732 ± 0.167	Random
G5597C	L	V289L	0.978 ± 0.025	1.030 ± 0.011	Random
G7128U	L	C799F	0.888 ± 0.036	0.635 ± 0.033	Random
C7287U	L	P852L	0.859 ± 0.026	0.681 ± 0.015	Random
U10809C	L	I2026T	0.997 ± 0.013	0.857 ± 0.014	39
U1323A/G7123C	N/L	F421L/none	1.041 ± 0.030	0.179 ± 0.015	Random
C2969A/U3192C	Intergenic/G	None/Y39H	0.894 ± 0.015	0.571 ± 0.037	Random
C3615A/U3192C	G/G	S180T/Y39H	0.619 ± 0.021	0.071 ± 0.017	Random
U3950G/C7287U	G/L	None/P852L	0.825 ± 0.039	0.225 ± 0.009	Random
G406T/U2617G	N/M	G115C/L123W	1.063 ± 0.088	1.038 ± 0.031	32
U2617G/A3802G	M/G	L123W/H242R	0.925 ± 0.034	1.170 ± 0.026	7, 32

[a] Nucleotide sites in the plus polarity Indiana genome (GenBank accession no. AM690336).
[b] Reference describing the substitution that was reproduced in this study.

mapping to the conserved C terminus of the N nucleoprotein (U1323A) had a strongly deleterious fitness effect but did not reduce or even slightly increased virulence, whereas a double mutation of the M matrix and G surface proteins (U2617G/A3802G) imparted high fitness yet relatively low virulence. These two mutants with unusual fitness-virulence relationships were further characterized in primary cultures from mouse brain cells and *in vivo*. The fitness effects observed in BHK-21 cells were reproducible in these more natural environments. In primary cultures, the virulence of these mutants depended on the infected cell type and on the mechanism of cell death (apoptosis or direct lysis). *In vivo*, the U2617G/A3802G double mutant showed reduced mortality rates, whereas the U1323A mutation had no effect on virulence despite its deleterious fitness effect.

MATERIALS AND METHODS

Cell culturing. BHK-21 cells were obtained from the American Type Culture Collection (www.atcc.org) and cultured in Dulbecco's modified Eagle's minimum medium (DMEM) (Invitrogen) supplemented with 9% fetal calf serum (FCS) at 37°C, 5% CO_2, and 95% relative humidity. Primary cortical cultures were prepared from newborn BALB/c mice. Pups were decapitated, and cerebral cortices were removed, fragmented, and collected in modified Eagle's medium (MEM) containing 10% FCS and 1% penicillin–streptomycin at 37°C. Tissue was rinsed with phosphate-buffered saline (PBS), incubated in trypsin (0.05%) at 37°C for 20 min, centrifuged to remove trypsin, resuspended in MEM with 10% FCS, and homogenized with a fire-polished Pasteur pipette. The homogenate was cleaned by centrifugation, resuspension in MEM, and filtration through 90-μm pores to remove large debris. Cells were resuspended in Neurobasal medium containing 2% B27 antioxidants, 1% L-glutamine, and 1% penicillin-streptomycin, plated over coverslips in flat-bottomed poly-L-lysine-coated 24-well plates, and incubated at 37°C, 5% CO_2, and 95% relative humidity. Cultures were cleaned by changing the medium every 2 days and infected at day 12.

Viruses. Our reference VSV clone was identical to the infectious clone originally created by Whelan et al. (45) except for an A-to-C substitution in position 3853 of the plus polarity RNA, which confers resistance to monoclonal antibody I_1 against the G surface glycoprotein (43), and was here designated MARM RSV. The 21 mutant viruses were derived from MARM RSV by site-directed mutagenesis as described in previous works (37, 38). Some of these mutants contained random nucleotide substitutions, whereas others reproduced substitutions found in the literature (Table 1). Original viral stocks were amplified once in BHK-21 cells at the start of this study to obtain enough titer, and one additional amplification step was carried out prior to *in vivo* assays. All titrations were done by the standard plaque assay in confluent BHK-21 monolayers under DMEM with 2% FCS solidified with 0.4% agarose.

BHK-21 cytotoxicity assays based on total cell surface areas. For each replicate assay, 10^4 cells at a confluence of <50% were inoculated with 3×10^4 PFU, the multiplicity of infection (MOI) thus being 3 PFU/cell. Since >95% of the cells were infected upon inoculation, only one infection cycle could take place. Thus, in these assays, viral cytotoxic effects should be independent of the speed at which virus infected the cells. At a lower MOI, the fastest-growing viruses would infect more cells per time unit and reduce the surface area of the culture more rapidly, thus making it more difficult to measure viral cytotoxicity independently from fitness. We infected 8 wells of a 96-well plate with each assayed virus and ran 8 mock-infected wells in parallel. Infected and control wells were incubated under identical conditions, and plates were stained at 16 h postinoculation (hpi) with 100 μl of 2% (wt/vol) crystal violet (Sigma) in 10% (vol/vol) formaldehyde. All assayed viruses should have completed an entire infection cycle at 16 hpi. Pictures were taken at minimum magnification in an Axiovert C25 inverted microscope (Zeiss) as recommended by the manufacturer. Each image corresponded to approximately 17% of the well and was analyzed using the AnalySIS software (Soft Imaging System) to determine the surface area occupied by cells. The same region was pictured in different wells to minimize the effects of nonuniform cell plating. The surface area occupied by cells in each infected well was divided by the average area of the uninfected controls, and cytotoxicity was quantified as the per-hour rate of change in this ratio.

BHK-21 cytotoxicity assays based on cell viability. In the cytotoxicity assays based on cell viability, cytotoxicity was estimated as the fraction of viable cells in infected wells relative to the average for the mock-infected control. To do so, 10^5 cells were inoculated with 3×10^5 PFU (MOI, 3 PFU/cell), and at 16 hpi, the fraction of viable cells on each well was determined by trypan blue staining using the Vi-CELL automated system. Three replicate wells per viral genotype were infected, and six mock-infected wells were run in parallel.

Cytotoxicity assays in primary cultures from mouse brain cells. Each well of a 24-well plate was inoculated with 1.5×10^5 PFU, and cells were fixed at 19 hpi with 4% paraformaldehyde (PFA) for 30 min at room temperature (r.t.), washed three times with PBS, and kept at 4°C in PBS with 0.1% azide until staining. For viability assays, cells were incubated 5 min with PBS containing 4 μg/μl propidium iodide (PI), 0.1% Triton X-100, and 0.5 mg/ml RNase A at r.t., washed three times with PBS, and fixed again as above. For *in situ* terminal deoxynucleotidyltransferase-mediated dUTP-biotin nick end labeling (TUNEL) apoptosis assays, the ApoTag fluorescein direct in situ kit (Millipore) was used according to the manufacturer's instructions. To stain neurons, cells were permeabilized with 0.2% % Triton X-100 in PBS. After blocking with 10% normal goat serum (NGS) in PBS containing 0.2% Triton X-100 for 1 h at r.t., cells were incubated with a 1:200 dilution of primary antibody Anti-β-tubulin III (Tuj-1) (Covance PRB435P) overnight at 4°C. The primary antibody was washed five times, and a 1:500 dilution of Alexa 647 goat anti-rabbit secondary antibody (A21245; Invitrogen) was added for 1 h at r.t. After another 5-fold wash with PBS and a distillate water rinse, slides were mounted with Vectashield solution with DAPI (4′,6-diamidino-2-phenylindole) (1.5 μg/ml). Slides were visualized and pictured at a magnification of ×40 in a Nikon fluorescence microscope, and images were analyzed with Photoshop software to count total cells (DAPI-positive nuclei), total dead cells (DAPI- and PI-positive nuclei), total apoptotic cells (DAPI- and TUNEL-positive nuclei), and the same subpopulations in neurons (Tuj-1 positive). For each of the three replicate assays, these counts were obtained from five random pictures.

Fitness assays in cell cultures. As detailed in previous work (38), each well containing 10^5 cells was inoculated with 5×10^3 PFU of the assayed mutant and the same amount of a common competitor. The latter was the original Whelan et al. virus (45), which is isogenic to MARM RSV but is sensitive to monoclonal antibody I_1. The titer of each competitor was determined at 12 hpi by plating in the presence and absence of the antibody, and growth rates were calculated as the per-hour increase in log titer. Fitness was expressed as the growth rate of the assayed mutant divided by that of the common competitor. Notice that for some of the mutants fitness was originally calculated in a different manner (37), but we converted all fitness values to growth rate ratios for consistency. Five replicate assays were performed for each mutant. The same procedure was followed for primary brain cultures, except that the estimated number of cells per well was 3.5×10^4 and that three replicate assays were performed.

Growth curves. We inoculated 10^5 cells with 5×10^3 PFU, determined viral titers at 6, 8, 10, 12, 14, 16, 20, 24, 30, and 40 hpi, and fit the following logistic growth model to the data:

$$\log N(t) = \log \frac{K}{1 + e^{c - rt}} \quad (1)$$

where N is the number of viruses relative to the total inoculated cells (PFU/10^5), t is time in hpi, K is the viral yield per cell (total viruses released per cell), r is the exponential growth rate (h^{-1}), and c sets the initial conditions. The duration of the eclipse phase or infection lag time was calculated as

$$L = \frac{1}{r}\left(c - \log \frac{K - N_i}{N_i}\right) \quad (2)$$

where $N_i = 5 \times 10^3/10^5 = 0.05$, which corresponds to the time at which the number of viruses released equals the inoculum size, N_i. As previously shown (8), the duration of a cell infection cycle (including the time required for transmission from one cell to another) can be calculated as $\tau = (\log K)/r$. Five replicate growth curves, model fits, and parameter estimations were carried out for each assayed virus. The same procedure was followed for primary cultures, but the estimated number of cells was 3.5×10^4 per well, three replicate assays were performed, and sampling times were 7.5, 9.5, 11.5, 13.5, 15.5, 20, 31.5, and 39.5 hpi.

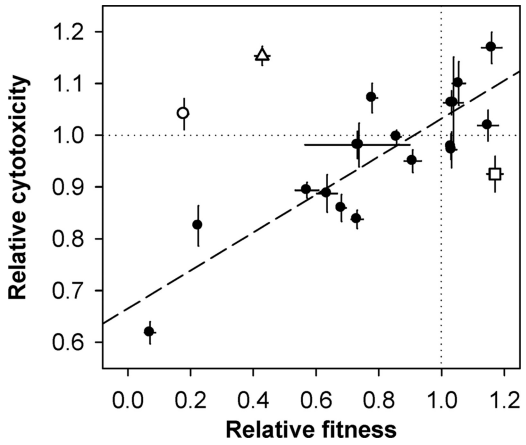

FIG 1 Fitness and virulence of VSV mutants in BHK-21 cells. Both variables are shown relative to the reference clone for each of the 21 mutants tested. Each data point corresponds to the average of eight cytotoxicity and five fitness replicate measurements, and bars indicate standard errors of the means (SEMs). The U1323A mutant is indicated by a triangle, the U1323A/G7123C mutant by a circle, and the U2617G/A3802G mutant by a square. The linear regression line obtained after excluding the first two mutants is shown as a dashed line. The dotted lines indicate the fitness and cytotoxicity values of the reference clone.

Mouse infections. Three-week-old BALB/c mice were inoculated intranasally with 10 μl of PBS containing the indicated number of PFU and observed for signs of disease such as dehydration, piloerection, weight loss, changes in behavior and body temperature, and hind limb paralysis. Animals were euthanized with pentobarbital at 4 days postinoculation for fitness assays and after 21 days for virulence assays. For fitness assays, brains were extracted and homogenized in cold PBS using a 2-ml Elvehjem tissue grinder (Bioblock Scientific), and viruses were titrated in BHK-21 monolayers in the presence and absence of I_1 antibody.

RESULTS

Correlation between fitness and virulence in BHK-21 cells. We characterized the relationship between viral fitness and virulence among 21 VSV mutants carrying one or two nucleotide substitutions relative to a common reference clone (Table 1). Fitness, defined as the per-hour rate of increase in log titer relative to a phenotypically marked common competitor, was obtained from previous works (37, 38) and varied significantly among mutants (one-way analysis of variance [ANOVA], $P < 0.001$). To quantify cytotoxicity, a proxy for virulence in cell cultures, we measured the rate at which the total surface area occupied by the culture decreased relative to uninfected controls. This was based on the fact that infected cells undergo virally induced apoptosis or direct lysis, thus detaching from the culture plate. We found that cytotoxicity varied significantly among the 21 mutants (one-way ANOVA, $P < 0.001$) and correlated positively with viral fitness (Fig. 1) (Pearson's $r = 0.516$; $P = 0.015$). However, some mutants appeared to deviate from this trend. The most obvious cases were the single-nucleotide U1323A mutant and the U1323A/G7123C double mutant. Both showed greatly reduced fitness compared

with the reference clone (t test, $P < 0.001$), but their cytotoxicity was unaffected or even slightly increased in the case of the U1323A mutant (t test, $P = 0.020$). A least-squares trimmed linear regression identified U1323A and U1323A/G7123C mutants as outliers, their cytotoxicity falling 2.4 and 1.9 standard deviations away from predicted values, respectively. Mutation U1323A produced the amino acid substitution F420L in the nucleocapsid protein N and was present in both outliers, whereas G7123C was a synonymous substitution that did not appear to contribute appreciably to the outlier phenotype.

The significance of the correlation between fitness and cytotoxicity strongly increased after removing the U1323A and U1323A/G7123C mutants from the data set ($r = 0.812$; $P < 0.001$). In contrast, removal of any other of the remaining 19 mutants had minor effects on the correlation ($0.690 \leq r \leq 0.864$; $P \leq 0.001$), thus indicating that the two mutants were well-defined outliers and that, after removing them, the relationship between fitness and cytotoxicity was robust. However, since the definition of an outlier depends on the underlying model assumed, we repeated the regression analysis using log-transformed fitness and cytotoxicity data. In log-log scale, the correlation between these two variables using all 21 mutants was also significant ($r = 0.635$; $P = 0.002$) and the linear regression gave a slope of 0.124 ± 0.034, suggesting that fitness increased less than linearly with cytotoxicity. The U1323A and U1323A/G7123C mutants were still clear outliers after this transforming, their cytotoxicity falling 2.2 and 2.3 standard deviations away from predicted values, respectively. Again, the correlation coefficient increased after removing these two data points ($r = 0.867$; $P < 0.001$) but did not change noticeably after removing any of the remaining 19 values.

Having isolated a low-fitness, high-cytotoxicity mutation, we sought mutants showing the opposite pattern, i.e., high fitness and low cytotoxicity. Although there were no obvious outliers of this kind, the U2617G/A3802G double mutant was significantly fitter than the reference clone (t test, $P = 0.002$) but slightly less cytotoxic. Furthermore, the double mutant showed lower cytotoxicity than expected from the effects of each single mutation alone (Table 1) (two-way ANOVA, $P = 0.019$), suggesting an interaction between the two amino acid replacements involved (L123W in the matrix protein M and H242R in the G glycoprotein). We therefore selected this double mutant for further characterization.

Characterization of U1323A and U2617G/A3802G mutants in BHK-21cells. Figure 2A shows plaque morphologies for U1323A and U2617G/A3802G mutants and the reference clone. The U1323A mutant formed small plaques, consistent with its low fitness, whereas the U2617G/A3802G mutant formed normal-sized yet turbid plaques, suggesting that cells were infected rapidly but were killed relatively inefficiently. Since the above competition assays were performed in the short term (12 hpi) and the estimated fitness of each mutant was thus determined mainly by its exponential growth rate, we performed growth curves over a 40-h interval to characterize fitness further (Fig. 2B). For comparison, the above fitness assays are shown in Fig. 2C. By fitting a logistic growth model to the data, we estimated the exponential growth rate, the lag (eclipse) time, the per-cell viral yield, and the duration of a cell infection cycle for each mutant and the reference clone (Table 2). Significant differences were found among these three viruses for each of the four estimated parameters (one-way ANOVA, $P \leq 0.044$). After doing all pairwise comparisons between viruses, we found that the U1323A mutant had a significantly longer lag time and a lower per-cell yield than the reference clone (Tukey's honestly significant difference [HSD] *post hoc* test, $P \leq 0.006$). The other two viruses grew similarly in the short term, but the final yield was more than twice as high for the reference clone as for the U2617G/A3802G mutant (HSD, $P = 0.047$). The lack of differences between their growth rates contrasts with the results of the competition assays but may simply reflect the greater accuracy of the latter assay to detect subtle fitness differences. The estimated duration of a cell infection cycle was shorter for the U2617G/A3802G mutant (HSD, $P = 0.003$), since it expanded rapidly in the culture (high growth rate) despite producing few infectious particles in each cell infection cycle. Considering the above results, we conclude

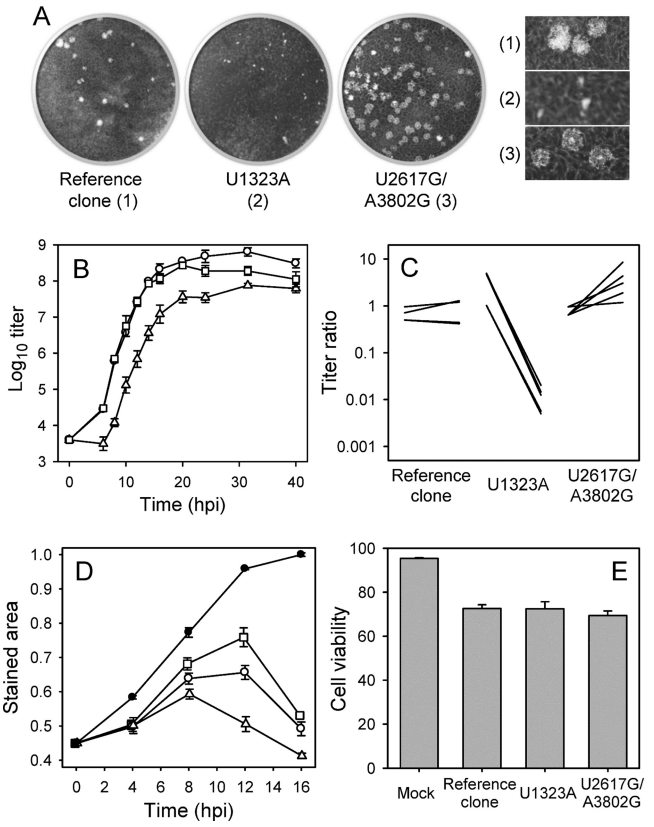

FIG 2 Fitness and virulence of selected mutants in BHK-21 cells. (A) Plaques of the reference clone, the U1323A mutant, and the U2617G/A3802G mutant. The inset pictures on the right side show representative plaque morphologies in greater detail for each of the three viruses. BHK-21 monolayers were stained with crystal violet at 30 hpi for the U1323A mutant and at 24 hpi for the other two viruses. (B) Growth curves of the reference clone (circles), the U1323A mutant (triangles), and the U2617G/A3802G mutant (squares). The average of five curves is shown for each virus, and error bars indicate standard errors of the means (SEMs). For each replicate, the data are well fitted by a logistic growth model ($r > 0.9$ in all cases). (C) Fitness assays of each of the three viruses against a common competitor. Lines represent the changes in titer ratio of the assayed virus to the common competitor from inoculation to sampling. The five replicates are shown for each virus. (D) Change in the total surface area of cultures infected with the reference clone (white circles), the U1323A mutant (white triangles), and the U2617G/A3802G mutant (white squares) and mock-infected cultures (black circles). Each data point corresponds to the average surface area of eight culture wells, and error bars indicate SEMs. Surface areas are in arbitrary units, the value 1.0 corresponding to the area of a confluent culture. (E) Average ($\pm$ SEM) cell viabilities in percentages determined by trypan blue staining.

TABLE 2 Fitness and virulence in BHK_{21} cells for selected mutants[a]

Characteristic	Reference clone	U1323A mutant	U2617G/A3802G double mutant
Fitness			
Relative fitness[b]	1.00 ± 0.001	0.429 ± 0.024	1.17 ± 0.03
Lag time, L (h)	4.54 ± 0.09	7.44 ± 0.37	4.77 ± 0.25
Exponential growth rate, r (h^{-1})	1.05 ± 0.03	0.890 ± 0.040	1.23 ± 0.14
Viral yield per cell, K (PFU)	2,189 ± 574	289 ± 75	840 ± 194
Length of cell infection cycle, τ (h)	7.21 ± 0.14	6.21 ± 0.11	5.58 ± 0.43
Virulence			
Relative cytotoxicity[b]	1.00 ± 0.05	1.15 ± 0.02	0.925 ± 0.034
Viability of infected cells (%)	72.6 ± 1.7	72.5 ± 3.2	69.4 ± 2.1

[a] Mean values ± SEM from five (fitness and growth curves), eight (relative cytotoxicity), and three (cell viability) replicate assays.
[b] Values from Table 1.

that, although the U2617G/A3802G mutant had a low per-cell yield, it retained a high fitness value probably because of its rapid cell-to-cell transmission rate. The low per-cell yield may in turn explain its relatively low cytotoxicity.

As indicated above, changes in the total surface area of infected BHK-21 cultures suggested that the U1323A mutant had slightly higher cytotoxicity than the reference clone, whereas the U2617G/A3802G mutant was less cytotoxic. Figure 2D shows these data in further detail. As a second measure of cytotoxicity, the viability of infected BHK-21 cells was determined by staining dead cells with trypan blue. Cell viability ranged from 69% to 73%, compared to 95% in uninfected controls (Fig. 2E; Table 2). The reference clone and the two mutants showed similar effects on viability (one-way ANOVA, $P = 0.586$) despite their different fitness values. It thus seems that the trypan blue assay was less sensitive in detecting differences in virus-induced cell damage. Conservatively, we can conclude that in BHK-21 cells, the U1323A mutant was as virulent as, or more virulent than, the reference clone, whereas the U2617G/A3802G double mutant was as virulent as, or less virulent than, the reference clone.

Fitness and virulence in primary cultures from mouse brain cells. To test whether the partial decoupling between fitness and cytotoxicity shown by the above mutants in BHK-21 cells could be reproduced in a more natural cellular environment, we performed growth curves, fitness assays, and cell viability tests in primary cultures of brain cells extracted from newborn BALB/c mice. The U1323A mutant showed impaired growth (Fig. 3A), whereas the U2617G/A3802G mutant and the reference clone reached similar titers. The exponential growth rate, lag time, per-cell viral yield, and duration of a cell infection cycle were estimated from each virus by fitting a logistic model to the growth curve data as above (Table 3). Pairwise comparisons showed that the U1323A mutant had a lower growth rate (HSD, $P \leq 0.003$) and per-cell viral yield ($P \leq 0.001$) than the other two viruses and a longer lag time ($P \leq 0.006$). This confirmed the growth defects exhibited by this mutant in BHK-21 cells. The U2617G/A3802G mutant appeared to have a slightly lower growth rate than the reference clone, although the difference was not statistically significant for this or any other of the growth parameters inferred (HSD, $P \geq 0.488$). Fitness assays were performed against a common, phenotypically marked competitor as above (Fig. 3B). Whereas for an equal input ratio with the common competitor the reference clone was recovered at a ratio of 0.732 ± 0.102, the U1323A mutant was recovered

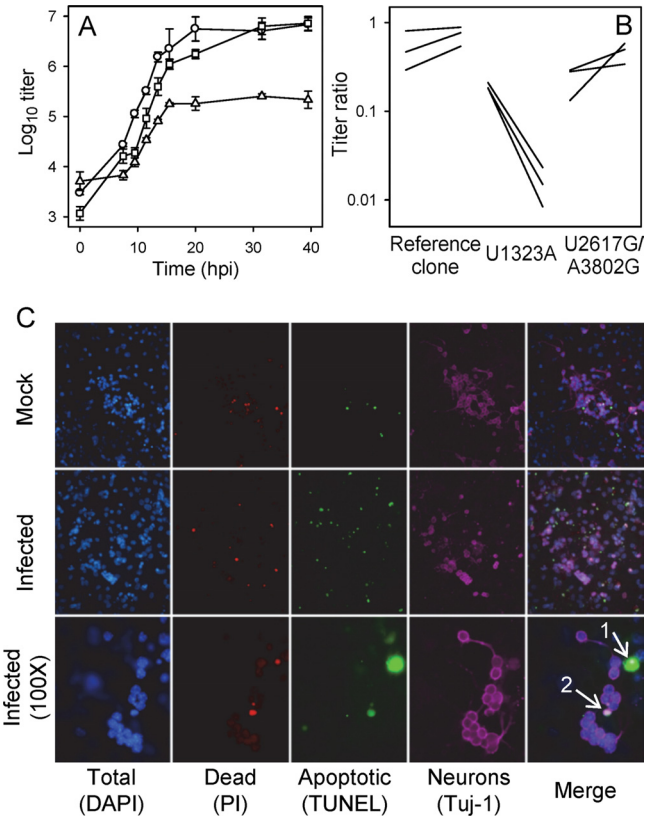

FIG 3 Fitness and virulence of selected mutants in primary cultures of brain cells from newborn mice. (A) Growth curves of the reference clone (circles), the U1323A mutant (triangles), and the U2617G/A3802G mutant (squares). The average of three curves is shown for each virus, and error bars indicate SEMs. (B) Fitness assays of each of the three viruses against a common competitor. Lines represent the changes in the titer ratio of the assayed virus to the common competitor from inoculation to sampling. The three replicates are shown for each virus. (C) Immunofluorescence images showing the effects of the virus on cellular viability and apoptosis. Nuclei from total, dead, and apoptotic cells were stained with DAPI, propidium iodide (PI), and the TUNEL assay, respectively. Neuron cytoplasms were marked with Tuj-1 antibody. A representative image is shown from one mock-infected control and a culture infected with the reference clone. Each count reported in Table 3 was based on 15 pictures (5 for each of the three replicate assays), each picture containing typically >100 DAPI-positive nuclei. The lower row of pictures shows a group of neurons surrounded by glial cells at a greater magnification (×100). Arrows 1 and 2 indicate one apoptotic/dead glial cell and one neuron, respectively.

TABLE 3 Fitness and virulence in primary cultures of brain cells from newborn mice for selected mutants[a]

Characteristic	Reference clone	U1323A mutant	U2617G/A3802G double mutant
Fitness			
Relative fitness[b]	1.00 ± 0.04	0.257 ± 0.060	1.08 ± 0.10
Lag time, L (h)	3.42 ± 0.17	8.01 ± 0.84	3.64 ± 0.62
Exponential growth rate, r (h^{-1})	0.468 ± 0.027	0.240 ± 0.019	0.428 ± 0.022
Viral yield per cell, K (PFU)	227 ± 105	9 ± 1	210 ± 56
Length of cell infection cycle, τ (h)	11.1 ± 0.4	9.5 ± 1.0	12.3 ± 0.9
Virulence			
Total cell viability (%)	89.1 ± 3.2	86.7 ± 1.1	91.3 ± 2.3
Apoptotic cells (%)	7.50 ± 1.67	4.61 ± 0.55	5.53 ± 0.78
Percent neurons	4.23 ± 0.66	5.89 ± 1.30	2.25 ± 0.71
Neuron viability (%)	70.3 ± 0.9	89.3 ± 3.3	83.8 ± 3.2
Apoptotic neurons (%)	1.56 ± 1.55	1.49 ± 1.49	9.97 ± 1.14

[a] Values are means ± SEMs from three replicate assays.
[b] Relative to the reference clone.

at a ratio of 0.016 ± 0.004 and thus was strongly deleterious, with a calculated fitness of 0.257 ± 0.060 relative to the reference clone (Table 3) (t test, $P = 0.006$). In contrast, the U2617G/A3802G mutant showed slightly higher fitness than the reference clone, although it did not significantly deviate from neutrality (t test, $P = 0.504$). Therefore, the growth parameters and fitness of each virus were in broad agreement with the results obtained in BHK-21 cells.

Viral cytotoxicity in primary cultures was quantified by immunofluorescence. Cell viability was determined using propidium iodide and DAPI to stain nuclei from dead and total cells, respectively (Fig. 3C). The total cell viability dropped from 96.9% ± 0.7% in uninfected controls to 87 to 91% in infected cultures. The U1323A mutant was slightly more cytotoxic than the reference clone, whereas the U2617G/A3802G mutant was less cytotoxic, although differences were not statistically significant (Table 3) (one-way ANOVA, $P = 0.434$). This result should reflect mainly the effects of the virus on glia, which were the predominant cell type in these cultures. Based on Tuj-1 immunostaining, neurons represented 7.64% ± 1.46% of total cells in uninfected controls and tended to be more severely affected by the infection than other cell types, although the effect depended on the virus. The strongest neurotoxic effect observed was that of the reference clone, which reduced viability from 91.7% ± 2.1% in uninfected controls to 70.3% ± 0.9%, its effect being significantly stronger than that of U1323A and U2617G/A3802G mutants (HSD, $P \leq 0.029$). We also quantified apoptosis by the TUNEL assay. In controls, 1.51% ± 0.14% of total cells and 0.46% ± 0.46% of neurons were TUNEL positive. For total cells, these percentages tended to increase in infected cultures, although we detected no significant differences among viruses (one-way ANOVA, $P = 0.252$). However, differences were found among neurons. The reference clone and the U1323A mutant triggered little or no apoptosis, whereas apoptosis levels were significantly increased in neurons infected with the U2617G/A3802G mutant (HSD, $P \leq 0.006$). We therefore conclude that cytotoxicity is dependent on the viral genotype, the cell type, and the cell death pathway. Overall, the three assayed viruses were similarly cytotoxic in primary cultures of newborn mouse brain cells, but the reference clone induced lysis more strongly in neurons, whereas the U2617G/A3802G mutant induced higher levels of neuron apoptosis.

Virulence and fitness in mice. We determined the fitness and virulence of the three above viruses in BALB/c mice. First, we performed a pilot experiment by intranasally inoculating mice with escalating doses of the reference clone ranging from 10^2 to 10^5 PFU. We found a dose-dependent effect of the virus on body weight (Fig. 4A), and we selected a dose of 4×10^4 PFU for subsequent experiments. Five replicate competition assays were performed for each of the three viruses (the reference clone and the U1323A and U2617G/A3802G mutants) by inoculating mice with 2×10^4 PFU of the assayed virus and the same amount of the phenotypically marked common competitor. Mice were euthanized at day 4, and brain homogenates were plated in the presence and absence of anti-G monoclonal antibody to determine the titer of each competitor. To check whether the initial mutations had reverted *in vivo*, supernatants from antibody-containing plates were harvested and used for sequencing the region of interest. For the U2617G/A3802G double mutant, this was successfully done for the five replicate assays, whereas for the U1323A mutant this was achieved in 4/5 replicates. We found that, in all cases, the initial mutations were preserved. The U2617G/A3802G mutant and the reference clone appeared to have similar fitness levels, although the former may be slightly deleterious (Fig. 4B; Table 4). The U1323A mutant was the most deleterious virus, consistent with the results obtained in cell cultures. However, the data showed too much variance within groups to detect significant differences among viruses (one-way ANOVA using log ratios, $P = 0.142$; Mann-Whitney nonparametric test, $P = 0.153$). Interestingly, though, the five mice coinfected with the U2617G/A3802G mutant and the common competitor were asymptomatic at day 4 and showed a nearly 10-fold average reduction in total brain titer compared with the other mice (Table 4) (Mann-Whitney test, $P = 0.040$). Therefore, the U2617G/A3802G mutant had a dominant suppressor effect on coinfecting viruses *in vivo*.

To quantify virulence, five mice were inoculated with 4×10^4 PFU of each virus, weighed daily for a week, and followed until day 21 to determine survival rates. Viruses affected differently the progression of body weight (one-way ANOVA controlling for time, $P = 0.001$). Whereas similar weight losses were observed for the reference clone and the U1323A mutant, the U2617G/A3802G mutant showed a significantly milder effect (HSD, $P \leq 0.005$) (Fig. 4C). Weight loss was accompanied by other symptoms such

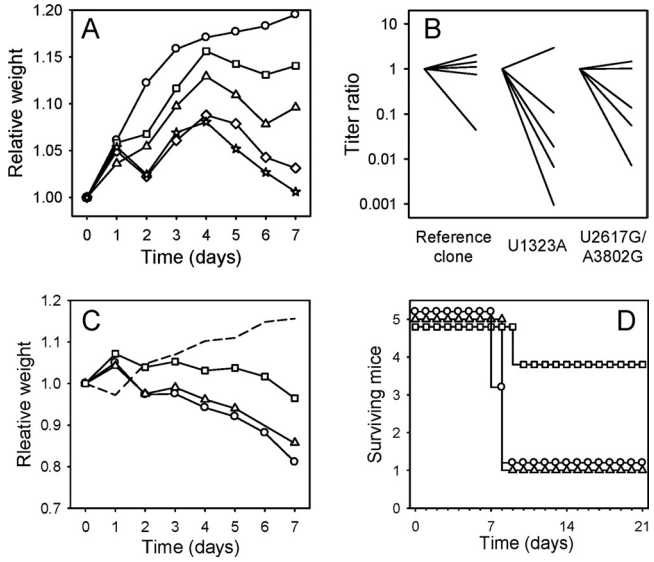

FIG 4 Fitness and virulence of selected mutants in mice. (A) Effects of escalating doses of the reference clone (circles, mock-infected controls; squares, 10^2 PFU; triangles, 10^3 PFU; diamonds, 10^4 PFU; stars, 10^5 PFU) on body weight. The values are relative to the initial weight and averaged over three mice per dose. Body weights tended to increase because mice were juvenile. (B) Fitness assays of the reference virus, the U1323A mutant, and the U2617G/A3802G mutant against a common competitor. Lines represent the changes in titer ratio of the assayed virus to the common competitor from inoculation to sampling. Initial ratios were 1:1 based on known titers but were not determined at inoculation. The five replicates are shown for each virus. (C) Changes in body weight of mice inoculated with 4×10^4 PFU of the reference clone (circles), the U1323A mutant (triangles), or the U2617G/A3802G mutant (squares). The average values from five mice are shown. The dashed line corresponds to uninfected controls. (D) Survival of mice infected with 4×10^4 PFU of the reference clone (circles), the U1323A mutant (triangles), or the U2617G/A3802G mutant (squares). To aid visualization, curves have been slightly shifted upwards or downwards.

as dehydration, piloerection, aggressiveness, sore ocular mucosa, and hind limb paralysis, and death followed starting on day 7 in 9/15 total infected mice. However, only 1/5 animals infected with the U2617G/A3802G mutant died after 21 days, whereas this fraction was 4/5 for those infected with the U1323A mutant or the reference clone (Fig. 4D; Table 4) (Breslow's generalized Wilcoxon test, $P = 0.036$). We thus conclude that the single mutation U1323A is probably deleterious *in vivo* but does not reduce virulence, whereas the double mutation U2617G/A3802G has a weak effect on relative fitness but produces significant viral attenuation.

DISCUSSION

Highly compact genomes such as those of VSV and most RNA viruses are highly sensitive to point mutations, and adaptation can be mediated by few substitutions (10, 22, 31). Therefore, it is not surprising that we found significant variation in both fitness and virulence among mutants carrying single or double nucleotide substitutions. The effects of mutations on viral fitness correlated positively with those on virulence in BHK-21 cells, but some mutations affected these two traits differentially. The clearest outlier was the single-nucleotide substitution U1323A, which was strongly deleterious for fitness yet did not reduce virulence in BHK-21 cells, a pattern that was reproducible in primary cultures from mouse brains and in infected mice. This mutation maps to the C terminus of the N protein, with a substitution at residue F420 in a conserved motif (SEFDK) that is required for assembly of a functional capsid (9, 46) and mediates interactions with the phosphoprotein P (42). It is therefore likely that the U1323A mutation impairs viral fitness by producing abnormal capsids with limited ability to support transcription and/or replication. The N protein forms a tunnel-like structure that wraps the viral genomic RNA and remains assembled during the entire infection cycle, shielding the viral RNA (16, 20, 33). Recent work showed, though, that conformational changes in the N protein make the RNA transiently accessible to other proteins to allow transcription and replication (19). Therefore, by changing the capsid structure, the U1323A mutation may also modify RNA-protein interactions, potentially altering host antiviral responses and producing greater cell damage than other similarly deleterious viruses.

At the within-host level, the U1323A mutant was rapidly outcompeted by faster-growing viruses, and although we did not test it, this mutant should also be selected against at the between-host level because it would not benefit from the greater transmissibility usually associated with extended host survival times. Therefore, poorly replicating yet virulent mutants such as the U1323A mutant should not be evolutionarily successful. In contrast, the combination of high within-host fitness and low virulence should be positively selected both at within-host and population levels. In BHK-21 cells, this combination was exhibited by the U2617G/A3802G double mutant. However, we cannot assess the likelihood of this type of combination to appear by chance because, in contrast to the U1323A mutation, the U2617G and A3802G mutations were not created randomly but, instead, reproduced changes reported previously in experimentally evolving lines (7, 32). Therefore, the number of random spontaneous mutations required to produce a high-fitness, low-virulence virus similar to the

TABLE 4 Fitness and virulence in mice for selected mutants[a]

Characteristic	Reference clone	U1323A mutant	U2617G/A3802G double mutant
Fitness			
Titer in brain (PFU/ml)	$(4.8 \pm 2.2) \times 10^5$	$(2.5 \pm 1.4) \times 10^4$	$(5.8 \pm 3.4) \times 10^4$
Titer of common competitor (PFU/ml)	$(6.9 \pm 3.2) \times 10^5$	$(1.3 \pm 1.1) \times 10^6$	$(9.2 \pm 3.2) \times 10^4$
Ratio of mean titers	0.696	0.019	0.630
Virulence			
Weight relative to controls	0.81 ± 0.04	0.75 ± 0.16	1.01 ± 0.02
No. of dead mice/total no.	4/5	4/5	1/5
No. of days to death	7, 7, 8, 8	8, 8, 8, 8	9

[a] Values are means ± SEM from five mice.

U2617G/A3802G mutant is probably greater than just a few tens. Furthermore, this mutant was only a weak outlier to the fitness-virulence relationship in BHK-21 cells, and its beneficial fitness effects were not confirmed in primary brain cultures or *in vivo*, further suggesting that it is not easy to simultaneously increase within-host fitness and reduce virulence.

The apparently host-dependent fitness of the U2617G/A3802G double mutant can be better understood in light of known molecular virus-host interactions. The U2617G mutation maps to protein M, which inhibits transcription, mRNA export to the cytoplasm, and translation and controls apoptosis (6, 17, 25, 35). Several mutations in this protein have been shown to modify virulence (36, 41). The A3802G mutation maps to protein G, which is also involved in interferon secretion, apoptosis, and pathogenicity (23, 24, 27, 28). Recent work in the field of oncolytic viruses has studied the properties of the U2617G/A3802G double mutant in the closely related Maraba virus (4). The mutant was attenuated in primary human fibroblasts and in mice but replicated fast and was highly cytotoxic in several tumoral cell lines. While the contribution of mutation A3802G is unclear, mutation U2617G was shown to impair the ability of protein M to block the expression of β interferon. This is consistent with our finding that neurons infected with the U2617G/A3802G mutant showed higher levels of apoptosis than those infected with the nonmutated virus, since interferon secretion promotes apoptosis. Given that apoptosis is part of the innate antiviral response, it also explains why the U2617G/A3802G mutant is attenuated. Furthermore, this mutant had a suppressor effect on the reference clone, suggesting that the innate antiviral responses triggered against the U2617G/A3802G mutant inhibited the coinfecting viruses. Therefore, these mutations might be useful in the design of attenuated vaccines. In contrast, in many tumoral cells that are apoptosis resistant, the functional defect of the U2617G/A3802G mutant is of little consequence (4). BHK-21 cells are quasitumoral, immortalized cells and do not mount an effective interferon response (2, 30). Hence, the slightly attenuated phenotype of this mutant may be determined by other factors.

In sum, although we found a positive correlation between fitness and virulence among VSV mutants in a simple cell culture system, the U1323A and U2617G/A3802G mutants deviated from this trend, and this partial fitness-virulence decoupling was reproducible in primary cultures and *in vivo*. However, the mechanisms underlying fitness and virulence may be specific to each studied system. For instance, the inability to block apoptosis and the associated antiviral responses was probably one mechanism underlying the low virulence of the U2617G/A3802G mutant *in vivo* but presumably not in BHK-21 cells. This impairment may be also responsible for the low accumulation levels of this mutant *in vivo* but did not severely diminish its competitive ability because antiviral responses may also inhibit coinfecting viruses. Therefore, our results show that viral fitness and virulence have complex determinants and can be influenced by cell type specificities and virus-virus interactions.

ACKNOWLEDGMENTS

R.S. was financially supported by grant BFU2008-03978, grant BFU2011-25271, the Ramón y Cajal research program from the Spanish MICINN, and Starting Grant 2011-281191 from the European Research Council (ERC). J.C.B. was supported by grants from the Ontario Institute for Cancer Research and the Terry Fox Foundation. V.F. was supported by a Ph.D. fellowship from MICINN.

We thank José Manuel García-Verdugo, Mónica Ramírez-Ruano, and Regina Rodrigo for helpful advice and comments.

REFERENCES

1. **Alizon S, Hurford A, Mideo N, Van BM.** 2009. Virulence evolution and the trade-off hypothesis: history, current state of affairs and the future. J. Evol. Biol. **22**:245–259.
2. **Andzhaparidze OG, Bogomolova NN, Boriskin YS, Bektemirova MS, Drynov ID.** 1981. Comparative study of rabies virus persistence in human and hamster cell lines. J. Virol. **37**:1–6.
3. **Bilsel PA, Nichol ST.** 1990. Polymerase errors accumulating during natural evolution of the glycoprotein gene of vesicular stomatitis virus Indiana serotype isolates. J. Virol. **64**:4873–4883.
4. **Brun J, et al.** 2010. Identification of genetically modified Maraba virus as an oncolytic rhabdovirus. Mol. Ther. **18**:1440–1449.
5. **Carrasco P, de la Iglesia F, Elena SF.** 2007. Distribution of fitness and virulence effects caused by single-nucleotide substitutions in Tobacco Etch virus. J. Virol. **81**:12979–12984.
6. **Connor JH, Lyles DS.** 2002. Vesicular stomatitis virus infection alters the eIF4F translation initiation complex and causes dephosphorylation of the eIF4E binding protein 4E-BP1. J. Virol. **76**:10177–10187.
7. **Cuevas JM, Elena SF, Moya A.** 2002. Molecular basis of adaptive convergence in experimental populations of RNA viruses. Genetics **162**:533–542.
8. **Cuevas JM, Moya A, Sanjuán R.** 2005. Following the very initial growth of biological RNA viral clones. J. Gen. Virol. **86**:435–443.
9. **Das T, Chakrabarti BK, Chattopadhyay D, Banerjee AK.** 1999. Carboxy-terminal five amino acids of the nucleocapsid protein of vesicular stomatitis virus are required for encapsidation and replication of genome RNA. Virology **259**:219–227.
10. **Domingo E.** 2006. Quasispecies: concept and implications for virology. Springer, Berlin, Germany.
11. **Duffy S, Holmes EC.** 2008. Phylogenetic evidence for rapid rates of molecular evolution in the single-stranded DNA begomovirus tomato yellow leaf curl virus. J. Virol. **82**:957–965.
12. **Ebert D.** 1998. Experimental evolution of parasites. Science **282**:1432–1435.
13. **Frank SA, Schmid-Hempel P.** 2008. Mechanisms of pathogenesis and the evolution of parasite virulence. J. Evol. Biol. **21**:396–404.
14. **Fraser C, Hollingsworth TD, Chapman R, de Wolf F, Hanage WP.** 2007. Variation in HIV-1 set-point viral load: epidemiological analysis and an evolutionary hypothesis. Proc. Natl. Acad. Sci. U. S. A. **104**:17441–17446.
15. **Gallione CJ, Greene JR, Iverson LE, Rose JK.** 1981. Nucleotide sequences of the mRNA's encoding the vesicular stomatitis virus N and NS proteins. J. Virol. **39**:529–535.
16. **Ge P, et al.** 2010. Cryo-EM model of the bullet-shaped vesicular stomatitis virus. Science **327**:689–693.
17. **Glodowski DR, Petersen JM, Dahlberg JE.** 2002. Complex nuclear localization signals in the matrix protein of vesicular stomatitis virus. J. Biol. Chem. **277**:46864–46870.
18. **Gopalakrishna Y, Lenard J.** 1985. Sequence alterations in temperature-sensitive M-protein mutants (complementation group III) of vesicular stomatitis virus. J. Virol. **56**:655–659.
19. **Green TJ, et al.** 2011. Access to RNA encapsidated in the nucleocapsid of vesicular stomatitis virus. J. Virol. **85**:2714–2722.
20. **Green TJ, Zhang X, Wertz GW, Luo M.** 2006. Structure of the vesicular stomatitis virus nucleoprotein-RNA complex. Science **313**:357–360.
21. **Herrera M, García-Arriaza J, Pariente N, Escarmís C, Domingo E.** 2007. Molecular basis for a lack of correlation between viral fitness and cell killing capacity. PLoS Pathog. **3**:e53. doi:10.1371/journal.ppat.0030053.
22. **Holmes EC.** 2009. The evolution and emergence of RNA viruses. Oxford University Press, Oxford, England.
23. **Ito N, Takayama M, Yamada K, Sugiyama M, Minamoto N.** 2001. Rescue of rabies virus from cloned cDNA and identification of the pathogenicity-related gene: glycoprotein gene is associated with virulence for adult mice. J. Virol. **75**:9121–9128.
24. **Janelle V, Brassard F, Lapierre P, Lamarre A, Poliquin L.** 2011. Mutations in the glycoprotein of vesicular stomatitis virus affect cytopathogenicity: potential for oncolytic virotherapy. J. Virol. **85**:6513–6520.
25. **Lyles D, Rupprecht CE.** 2006. Rhabdoviridae, p 1363–1408. *In* Knipe

DM, Howley PM (ed), Fields virology. Lippincott, Williams and Wilkins, Philadelphia, PA.
26. **Martín J, Minor PD.** 2002. Characterization of CHAT and Cox type 1 live-attenuated poliovirus vaccine strains. J. Virol. **76**:5339–5349.
27. **Martínez I, Rodríguez LL, Jiménez C, Pauszek SJ, Wertz GW.** 2003. Vesicular stomatitis virus glycoprotein is a determinant of pathogenesis in swine, a natural host. J. Virol. **77**:8039–8047.
28. **Morimoto K, Hooper DC, Spitsin S, Koprowski H, Dietzschold B.** 1999. Pathogenicity of different rabies virus variants inversely correlates with apoptosis and rabies virus glycoprotein expression in infected primary neuron cultures. J. Virol. **73**:510–518.
29. **Morita K, Vanderoef R, Lenard J.** 1987. Phenotypic revertants of temperature-sensitive M protein mutants of vesicular stomatitis virus: sequence analysis and functional characterization. J. Virol. **61**:256–263.
30. **Nagai Y, Ito Y, Hamaguchi M, Yoshida T, Matsumoto T.** 1981. Relation of interferon production to the limited replication of Newcastle disease virus in L cells. J. Gen. Virol. **55**:109–116.
31. **Novella IS.** 2003. Contributions of vesicular stomatitis virus to the understanding of RNA virus evolution. Curr. Opin. Microbiol. **6**:399–405.
32. **Novella IS, Hershey CL, Escarmís C, Domingo E, Holland JJ.** 1999. Lack of evolutionary stasis during alternating replication of an arbovirus in insect and mammalian cells. J. Mol. Biol. **287**:459–465.
33. **Ostertag D, Hoblitzell-Ostertag TM, Perrault J.** 2007. Overproduction of double-stranded RNA in vesicular stomatitis virus-infected cells activates a constitutive cell-type-specific antiviral response. J. Virol. **81**:503–513.
34. **Pagán I, Alonso-Blanco C, García-Arenal F.** 2007. The relationship of within-host multiplication and virulence in a plant-virus system. PLoS One **2**:e786. doi:10.1371/journal.pone.0000786.
35. **Petersen JM, Her LS, Varvel V, Lund E, Dahlberg JE.** 2000. The matrix protein of vesicular stomatitis virus inhibits nucleocytoplasmic transport when it is in the nucleus and associated with nuclear pore complexes. Mol. Cell. Biol. **20**:8590–8601.
36. **Publicover J, Ramsburg E, Robek M, Rose JK.** 2006. Rapid pathogenesis induced by a vesicular stomatitis virus matrix protein mutant: viral pathogenesis is linked to induction of tumor necrosis factor alpha. J. Virol. **80**:7028–7036.
37. **Sanjuán R, Moya A, Elena SF.** 2004. The contribution of epistasis to the architecture of fitness in an RNA virus. Proc. Natl. Acad. Sci. U. S. A. **101**:15376–15379.
38. **Sanjuán R, Moya A, Elena SF.** 2004. The distribution of fitness effects caused by single-nucleotide substitutions in an RNA virus. Proc. Natl. Acad. Sci. U. S. A. **101**:8396–8401.
39. **Schubert M, Harmison GG, Meier E.** 1984. Primary structure of the vesicular stomatitis virus polymerase (L) gene: evidence for a high frequency of mutations. J. Virol. **51**:505–514.
40. **Stewart AD, Logsdon JM, Jr, Kelley SE.** 2005. An empirical study of the evolution of virulence under both horizontal and vertical transmission. Evolution **59**:730–739.
41. **Stojdl DF, et al.** 2003. VSV strains with defects in their ability to shutdown innate immunity are potent systemic anti-cancer agents. Cancer Cell **4**:263–275.
42. **Takacs AM, Das T, Banerjee AK.** 1993. Mapping of interacting domains between the nucleocapsid protein and the phosphoprotein of vesicular stomatitis virus by using a two-hybrid system. Proc. Natl. Acad. Sci. U. S. A. **90**:10375–10379.
43. **Vandepol SB, Lefrancois L, Holland JJ.** 1986. Sequences of the major antibody binding epitopes of the Indiana serotype of vesicular stomatitis virus. Virology **148**:312–325.
44. **Vignuzzi M, Wendt E, Andino R.** 2008. Engineering attenuated virus vaccines by controlling replication fidelity. Nat. Med. **14**:154–161.
45. **Whelan SP, Ball LA, Barr JN, Wertz GT.** 1995. Efficient recovery of infectious vesicular stomatitis virus entirely from cDNA clones. Proc. Natl. Acad. Sci. U. S. A. **92**:8388–8392.
46. **Zhang X, Green TJ, Tsao J, Qiu S, Luo M.** 2008. Role of intermolecular interactions of vesicular stomatitis virus nucleoprotein in RNA encapsidation. J. Virol. **82**:674–682.